ANL/NSE-19/46

Recent SAM Code Improvement to Heat Transfer Modeling Capabilities

Nuclear Science and Engineering Division

About Argonne National Laboratory
Argonne is a U.S. Department of Energy laboratory managed by UChicago Argonne, LLC under contract DE-AC02-06CH11357. The Laboratory's main facility is outside Chicago, at 9700 South Cass Avenue, Argonne, Illinois 60439. For information about Argonne and its pioneering science and technology programs, see www.anl.gov.

ANL-NSE-19/46

Recent SAM Code Improvement to Heat Transfer Modeling Capabilities

prepared by
Ling Zou and Rui Hu
Nuclear Science and Engineering Division, Argonne National Laboratory

December 2019

EXECUTIVE SUMMARY

System Analysis Module (SAM) is currently under development at Argonne National Laboratory as a modern system-level modeling and simulation tool for advanced non-light water reactor (non-LWR) safety analyses. It utilizes the object-oriented application framework MOOSE to leverage the modern software environment and advanced numerical methods. The capabilities of SAM are being extended to enable the transient modeling, analysis, and design of various advanced nuclear reactor systems.

This report summarizes recent SAM code improvement to heat transfer modeling capabilities to support system and core thermal-hydraulics analysis for advanced nuclear reactor systems. These new capabilities include implementation of the energy equation for solid structure in porous medium and its coupling with porous medium flow energy equation; coupling between one-dimensional flow equation and three-dimensional heat conduction equation; coupling between two-dimensional heat structure and three-dimensional porous medium flow equations; and implementation of effective thermal conductivity correlations for solid pebble beds and its validation against High Temperature Test Unit (HTTU) experimental data. Demonstration or validation test problems are also included in this report to confirm the successful implementation of these capabilities.

Table of Contents

LIST OF FIGURES

LIST OF TABLES

1 Introduction

The System Analysis Module (SAM) is a modern system analysis code being developed at Argonne National Laboratory for advanced non-light water reactor (non-LWR) safety analysis [1]. SAM code development has attracted a wide range of interests from the advanced non-LWR community, and recently, U.S. Nuclear Regulatory Commission (U.S. NRC) also stated its intent to use SAM as the system and core thermal-hydraulics analysis code for design basis events of advanced non-LWRs [2].

Compared to existing light water reactor designs, advanced non-LWR concepts are different in many ways, including, for example, the choose of reactor core coolant and fuel form, core configurations, etc. In terms of system and core thermal-hydraulics analysis, it requires additional capabilities to consider multi-scale, multi-dimensional, and multi-physics effects that are typical for advanced non-LWR designs. To address these modeling and simulation challenges, it is necessary to improve SAM code, especially in areas such as multi-scale and multi-dimensional heat transfer modeling capabilities. This report summarizes recent such code improvements to heat transfer modeling capabilities. These new capabilities include the implementation of energy equation for solid structure in porous medium and its coupling with porous medium flow equations; coupling between one-dimensional flow equation and three-dimensional heat conduction equation; coupling between two-dimensional heat structure and three-dimensional porous medium flow equations; and implementation of effective thermal conductivity models of solid pebble beds and its validation against High Temperature Test Unit (HTTU) experimental data.

2 Solid Energy Equation in Porous Medium Flow Applications

In nuclear reactor thermal-hydraulics analysis, it is a common approach to using porous medium flow to model the fluid flow and heat transfer in very complex but with regular pattern geometries, such as the pebble bed core in high temperature gas-cooled reactors (HTGRs) and tube bundles in steam generators. As such examples, THERMIX [3] and recently developed Pronghorn [4] are both based on porous-medium approach and are used to predict core thermal-hydraulics behaviors in pebble-bed type of reactors. The COMMIX code [5][6] was based on multiphase porous medium approach, which had been successfully applied in many thermal-hydraulics analysis applications, such as reactor rod bundles and heat exchangers. CUPID-SG, a derivative of CUPID, is also such an example that uses a porous medium approach for thermal-hydraulics analysis of pressurized water reactor (PWR) steam generators [7].

In SAM, a similar porous medium flow model capability has been recently developed to support the modeling and simulation needs for flow and heat transfer in complex geometries, such as pebble beds. The model is intended to model single-phase flow in porous medium and its heat transfer with the solid structures. The implementation of the porous medium flow model is based on an existing 3D flow model previously implemented in SAM [8]. This 3D flow model was implemented in its conservative form, and has recently been updated to also include its primitive form, such that a unified 3D flow and porous medium flow model could be further developed.

For the porous medium flow model, the following equations describe the mass, momentum, and energy balance of the fluid phase:

$$\varepsilon\frac{\partial\rho}{\partial t}+\nabla\cdot(\rho\vec{v})=0 \tag{2.1}$$

$$\rho\frac{\partial\vec{v}}{\partial t}+\frac{\rho}{\varepsilon}(\vec{v}\cdot\nabla)\vec{v}+\varepsilon\nabla p-\varepsilon\rho\vec{g}+\alpha\vec{v}+\beta|\vec{v}|\vec{v}=0 \tag{2.2}$$

$$\varepsilon\rho c_p\frac{\partial T}{\partial t}+\rho c_p\vec{v}\cdot\nabla T-\nabla\cdot(\varepsilon k\nabla T)-q'''+a_w h(T-T_s)=0 \tag{2.3}$$

An addition solid energy equation is added to describe heat conduction within solid structure and its convective heat transfer with the fluid phase:

$$(1-\varepsilon)\rho_s c_{p,s}\frac{\partial T_s}{\partial t}-\nabla\cdot\left(k_{eff}\nabla T_s\right)+a_w h(T_s-T)-q_s'''=0 \tag{2.4}$$

In equations above, ε is the porosity of the porous medium, $\vec{v}$ is the so-called superficial veloc- ity, which is related to the intrinsic velocity, $\vec{V}$, as $\vec{v}=\vec{V}\varepsilon$. The last two terms in the left-hand-side of equation (2.2) represent the viscous and inertia terms, respectively. Currently, several empirical correlations have been implemented in SAM for the two coefficients, α and β. The heat transfer between the fluid and solid phase is represented by the $a_w h(T-T_s)$ term in the fluid energy equation (2.3), as well as the $a_w h(T_s-T)$ term in the solid energy equation (2.4), in which a_w is heat transfer area per unit volume. Again, empirical correlations are available for the heat transfer coefficient h, such as the KTA correlation [9] for high temperature gas-cooled reactors.

In the remaining of this section, two simple test problems are provided to demonstrate this newly added code capability. The first test problem is rather simple in terms of geometry, which is a 2D rectangle domain in the Cartesian coordinates, as shown in Figure 1. Both the flow equations and solid energy equation, i.e., equations (2.1)-(2.4), are simultaneously solved in this domain. Boundary conditions and other input parameters such as the volumetric heat source in the solid phase is also shown in Figure 1. SAM simulation was performed using a uniform 20(x)×8(y) mesh size, from which steady-state solutions were obtained.

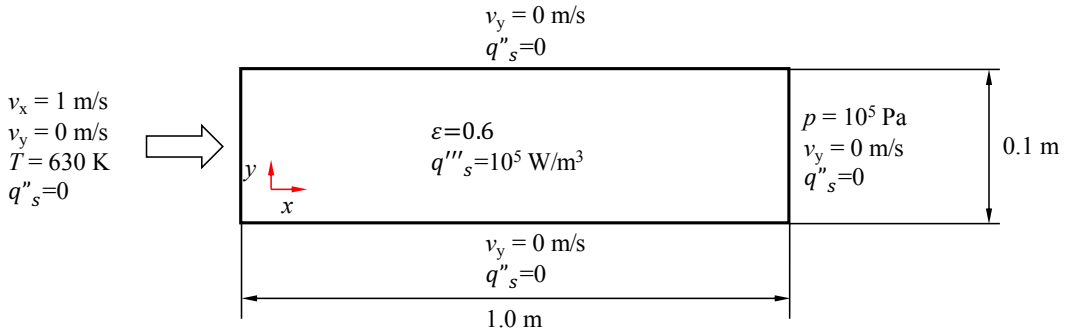

Figure 1, Simulation domain and boundary conditions for the first test case on coupled solid energy equation to porous medium flow equations.

The steady-state SAM simulation results are shown in Figure 2 for fluid temperature, solid temperature, and fluid velocity magnitude. The fluid and solid temperatures along the center line of the domain (y=0.05m) are also plotted in Figure 3. Although the problem setup seems quite simple, there does not exist analytical solutions for verification purpose. Nevertheless, it can be observed that the liquid temperature increases almost linearly with x-location due to energy transferring from the solid phase to it. For the solid phase temperature, its distribution is more complex than a simple linear one as a result of volumetric heat source, heat transfer to the liquid phase, as well as heat conduction within the solid phase. The fluid velocity also shows a correct trend that it increases with x-location as a result of increasing temperature (decreasing density). As a minimum verification effort, energy balance between the heat generation in the solid phase and the heat removal to the liquid phase has been computed, and it was found a well energy balance could be reached.

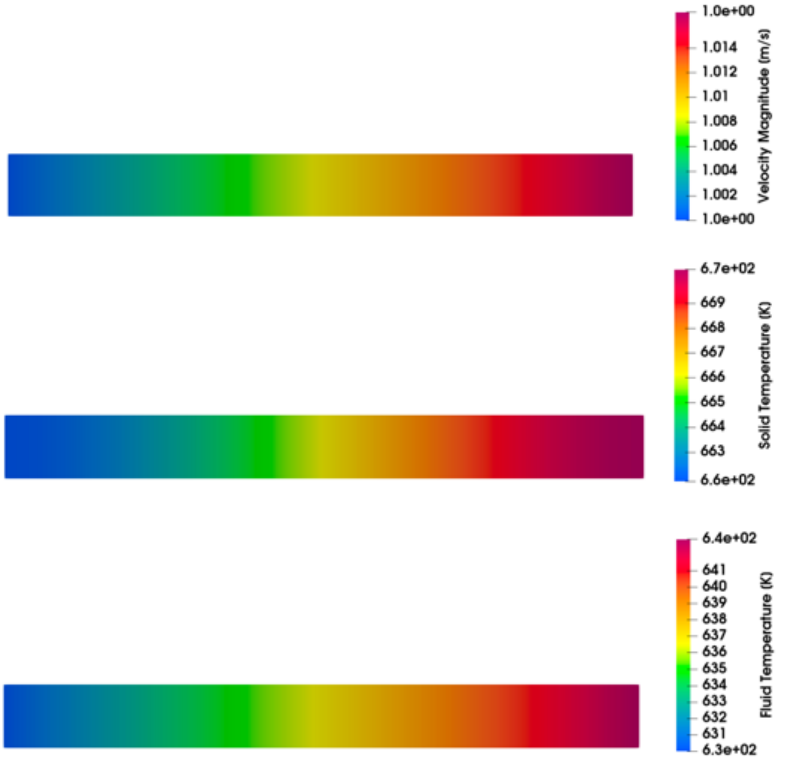

Figure 2, SAM results for the first test problem on coupled solid energy equation to porous medium flow equations in a 2D rectangle domain. Top: fluid temperature; Middle: solid temperature; Bottom: velocity magnitude.

A second test problem was then constructed to demonstrate such fluid-to-solid heat transfer capability in a more complex geometry, with a cavity-pebble bed-cavity configuration in a 3D domain. As shown in Figure 4, coolant flows into the domain from the bottom surface and leaves from the top surface. From bottom to top, there are three consecutive blocks of cavity, pebble bed, and cavity. In both cavity blocks, the porosity is set to be 1, and there is no solid structure present. Therefore, there is no solid temperature, and therefore solid energy equation, solved in the two cavity domains. In the center porous bed block, the porosity is set to be 0.4,

and solid temperature is solved from the solid energy equation. Such a configuration is similar to those of pebble bed reactors where upper and lower plenum could be modeled as cavities while the reactor core modeled using the porous media flow equations. For this test problem, the volumetric heat source in the pebble bed takes the form of,

$$q_s''' = 5 \times 10^7 \cos\left(\frac{\pi\sqrt{x^2+y^2}}{4}\right)\cos\left(\frac{\pi z}{8}\right)$$

which does not have physical importance, while the sole purpose is to demonstrate the multi-dimensional effect of the simulation.

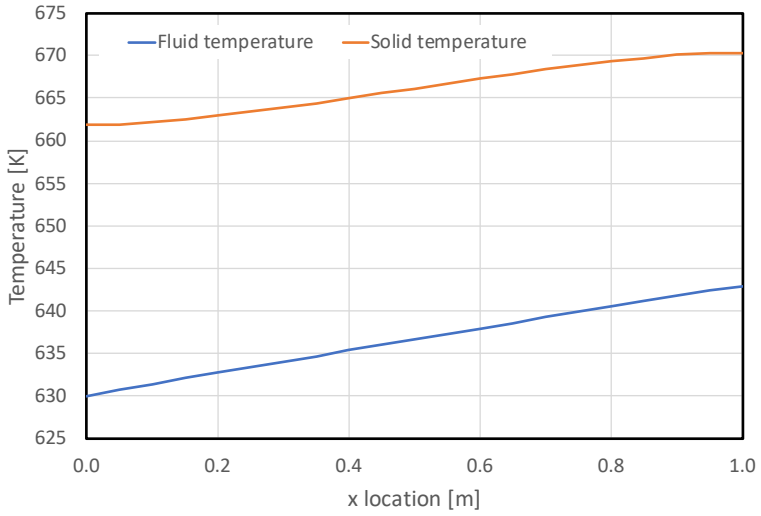

Figure 3, Fluid and solid temperature plots of the first test problem on coupled solid energy equation to porous medium flow equations in a 2D rectangle domain.

SAM steady-state results are shown in Figure 5. Similar to the previous test problem, the liquid temperature increases along its flow path as it picks up the heat from the solid phase. The solid temperature shows a more complex distribution as a result of the central peaked power distribution, heat transferring to the liquid, as well as the heat conduction within the pebble bed. The right plot in Figure 5 shows the fluid velocity distribution in the entire domain. As we have intentionally chosen the so-called superficial velocity to solve, the velocity transition across the cavity-to-pebble bed interface is smooth. Otherwise, if the intrinsic velocity had been chosen, there would be a sudden jump in velocity magnitude due to the sudden change of porosity, which could be generally problematic for FEM-based computer code, such as SAM.

As a brief summary for this section, the energy equation for solid phase in porous medium has been added into SAM, and coupled to the porous medium flow equations. Two test problems were included to demonstrate this newly added capability. The first problem uses a fairly simple 2D rectangle geometry while the energy balance could be easily verified. The second problem takes place in a more complex 3D domain with a cavity-pebble bed-cavity configuration, and spatially non-uniform heat source was applied in the pebble bed. For both

problems, it has been demonstrated that SAM has the capability and flexibility to handle complex heat transfer problems in pebble bed reactor type of applications.

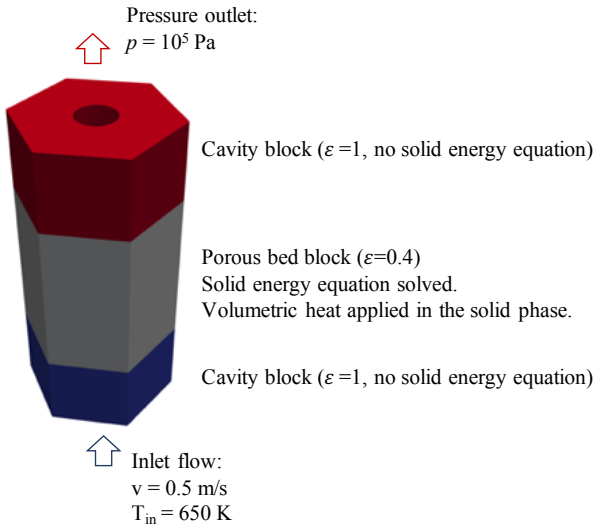

Figure 4, Problem setup for the second test case in a 3D domain with cavity-pebble bed-cavity blocks. Solid energy equation is only solved in the pebble bed block with a given volumetric heat source.

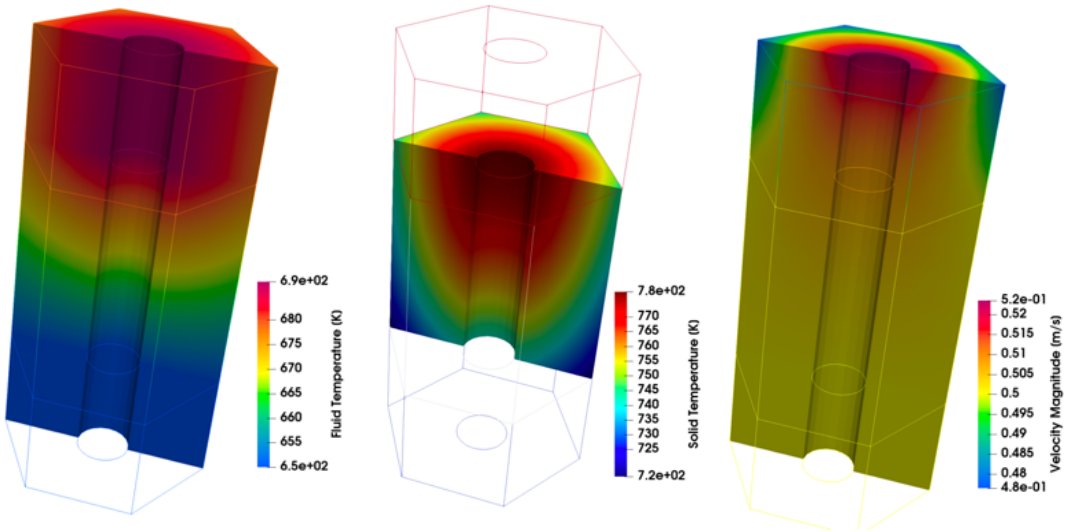

Figure 5, SAM results for the second test problem in a 3D domain. Left: fluid temperature; Middle: solid temperature; Right: velocity magnitude.

3 Coupling between 1D Flow and 3D Solid Heat Conduction

In traditional system analysis approaches, it is typical to treat heat conduction in solid structures using one- or two-dimensional heat conduction equation. This is partially due to the difficulty to generate unstructured three-dimensional mesh in such tools, and also partially due to the large computational cost associated with solving such (then) large problems. For light water reactor applications, as fuel pins are more or less isolated from each other in terms of heat transfer, heat conduction in fuel pins could be appropriately modeled by one- or two-dimensional model for being axially symmetric. This is however not the case for some advanced reactor designs, where local symmetry is no longer valid. Heat conduction in hexagonal fuel block of modular high temperature gas-cooled reactor (MHTGR) designs and in fuel pebble bed of pebble bed reactor designs are such examples. On the other hand, using CFD type of modeling strategy for the entire fluid flow and solid structure domain is still expensive and not necessary. For many applications of interest to thermal-hydraulics analysis, fluid flow could still be modeled as one-dimensional flow, instead of being fully resolved using CFD tools. This not only reduces computational cost, but also improves simulation accuracy, as empirical correlations (such as pressure drop and heat transfer) could be easily used in one-dimensional flow models, while resolving them in CFD is expensive and not always reliable.

Currently, within SAM, the coupling between one-dimensional flow and three-dimensional heat conduction equation is realized by using MOOSE's built-in MultiApp capability. In this MultiApp setup, the heat conduction in three-dimensional mesh (the masterApp) and fluid flow equations in one-dimensional SAM flow channels (the subApp) are handled in separate input files. Data transfer between these two MOOSE App's are realized by using MOOSE's built-in MultiApp userObject transfer mechanism.

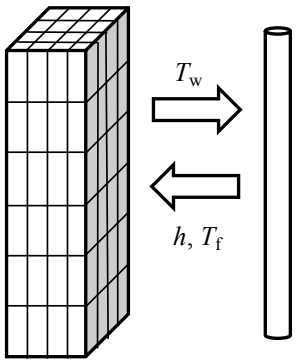

Figure 6, MultiApp setup to solve coupled one-dimensional fluid flow and three-dimensional heat conduction problem.

Figure 6 illustrates the MultiApp setup and data transfer mechanism for such a coupled one-dimensional fluid flow and three-dimensional heat conduction problem. As shown in Figure 6, conjugate heat transfer takes place between the right (gray) surface of the solid

structure and the 1D pipe. During iterations, area-averaged surface temperature from the masterApp, Tw, is computed using MOOSE's built-in 'LayeredSideAverage' UserObject, and then transferred to the subApp as 1D pipe's wall temperature using 'MultiAppUserObjectTransfer'. At the same time, convective heat transfer coefficient, h, and fluid temperature, T_f, are transferred to 3D heat conduction simulation, using 'MultiAppNearestNodeTransfer', to setup its boundary condition. Averaging process is not needed when transferring 1D flow data to 3D heat conduction simulations.

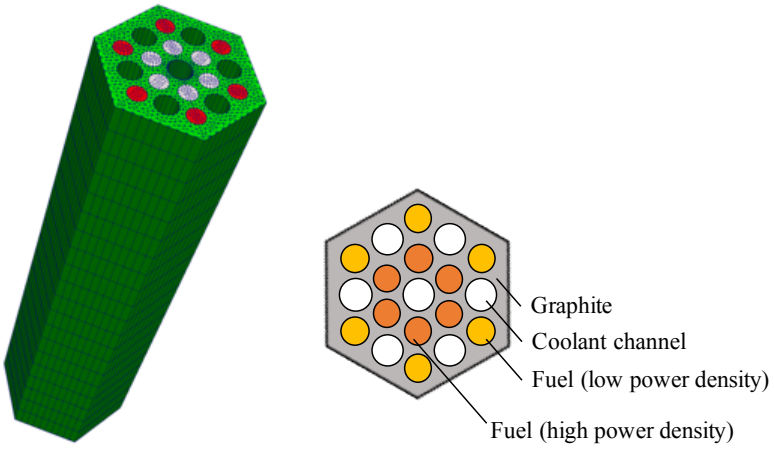

(a) (b)

Figure 7, Problem setup for the coupled 1D flow and 3D heat conduction simulation. (a) 3D mesh for heat conduction, (b) cross section of the 3D heat conduction problem.

A test case is given to demonstrate the 1D flow to 3D heat conduction coupling capability in SAM. Although it does not represent any real reactor design, the problem setup shown in Figure 7 mimics that of prismatic high temperature gas-cooled reactor designs. The solid structure consists of the hexagonal graphite block, 6 high power density fuel pins, and 6 low power density fuel pins. The block is 0.4m tall, and the flat-to-flat distance of its hexagonal cross section is 0.0954m. All fuel pins have the same diameter, which is 12.7 mm; and all coolant channels have the same diameter, 15.9mm. These input parameters are also summarized in Table 1.

Table 1 Input parameters for the coupled 1D flow and 3D heat conduction problem

Parameter	Value
# of high power density rods	6
Power density (high)	5×10^7 W/m^3
# of low power density rods	6
Power density (low)	3×10^7 W/m^3
Fuel rod diameter	12.7 mm
# of coolant channels	7
Coolant channel diameter	15.9 mm
Hexagonal block height	0.4 m
Hexagonal flat-to-flat distance	0.0954 m

As shown in Figure 7 (a), all solid structures are explicitly meshed, and the 3D heat conduction equation is solved in the masterApp. There are also 7 coolant channels in the graphite block, through which helium flows and carries heat away. These 7 coolant channels are modeled as 7 'PBOneDFluidComponent' in a separate subApp. The coolant is helium with an inlet velocity at 40m/s and temperature at 628.15K.

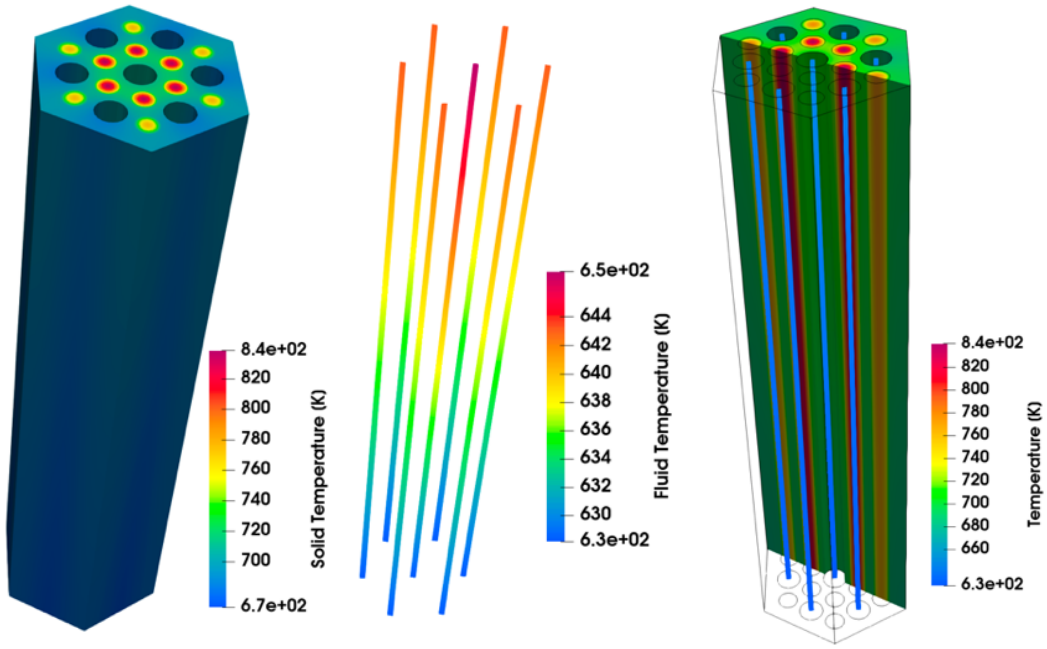

(a) (b) (c)

Figure 8, SAM simulation results: (a) solid temperature; (b) fluid temperature; (c) both solid and fluid temperatures.

Steady-state SAM simulation results are shown in Figure 8, and it is noted that the three sub plots have different temperature scales. The solid structure temperatures are shown in Figure 8 (a), with clearly highest temperatures in the high power density fuels. Figure 8 (b) shows the fluid temperatures in the 7 coolant channels. Fluid temperature increases from bottom (inlet) to top (outlet) as it picks up the heat generated in fuels. It is also clear that the central coolant channel has the highest outlet temperature, as it is surrounded by the 6 high power density fuel pins. Figure 8 (c) shows both the solid and fluid temperatures, as well as the positions of flow channels relative to solid structures.

Although a more rigorous verification and validation effort is beyond this current work scope, an energy balance calculation has been provided as a minimum level of assessment on this coupling approach. The total heat source is computed as the summation of all heat generated in each fuel rod, which is simply $\Sigma q_s''' V_{fuel}$, while the total heat removal is computed as the summation of the 7 coolant channels, which is $\Sigma \dot{m}(h_{out} - h_{in})$. It was found that the heat source and heat removal are well balanced from the steady-state solutions, with a relative error of 10^{-6}, within the convergence criteria.

4 2D Heat Structure and 3D Porous Medium Flow Coupling

In section 2, the newly added energy equation of solid phase in porous medium and its coupling to the porous medium flow equations has been successfully demonstrated. However, such a solid energy equation generally only concerns the 'surface' temperature of solid structures such as fuel pebbles. When, for example, the internal temperature distributions of pebbles are concerned, the approach described in section 2 is not able to provide such more detailed resolution. This is similar to the case when modeling the heat transfer between the condenser of heat pipes in a heat pipe- cooled reactor and the coolant flow in the heat exchanger. For such applications, the coolant flow in the heat exchanger could be modeled using the porous medium based flow model, however, heat conduction within heat pipes and the heat transfer between coolant flow and heat pipes also have to be explicitly modeled. This requires a more sophisticated modeling strategy than what has been presented in section 2. To overcome such a modeling and simulation difficulty, similar to the 1D flow coupling to 3D solid heat conduction presented in section 3, a multiApp strategy is developed. The porous medium flow equations are solved in the masterApp, which is able to handle complex geometry configuration, such as cavity-porous zone-cavity similar to that presented in section 2. The heat pipe problem is solved in the subApp, and the heat transfer between heat pipes and the coolant flow in the masterApp could be resolved by transferring data between the two App's. Such an example problem and mesh setup are illustrated in Figure 9.

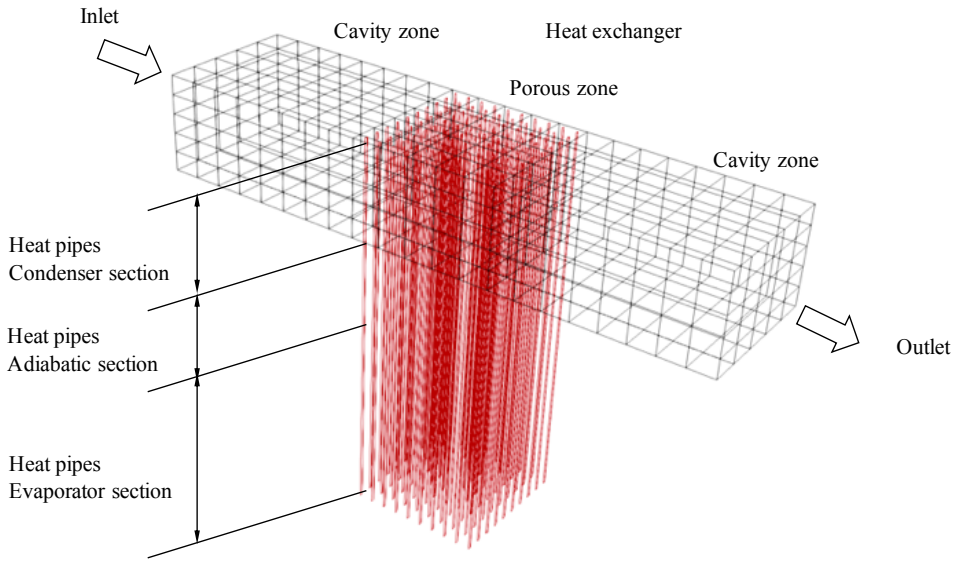

Figure 9, MultiApp setup to solve coupled 2D heat structure and 3D porous medium flow problem.

From Figure 9, it can be found that a quite coarse mesh setup is used for the coolant flow in the heat exchanger, and each cell contains several heat pipes within it. Such a mesh arrangement is based on the common practice that the mesh size in porous medium flow should be large enough to contain several heat structures, such that the porous medium flow

equation would make physical sense. This is similar to the case in pebble bed reactor simulations that the mesh size is normally large enough to contain multiple pebbles. A more detailed mesh setup for such a problem is illustrated in Figure 10, which shows a 'unit' cell that represents the entire porous zone domain shown in Figure 9.

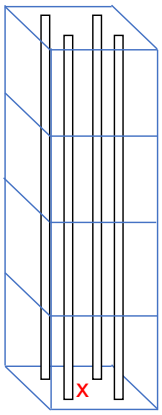

Figure 10, A 'unit' mesh setup for the 2D heat structure coupling with 3D porous medium flow problem. The blue cubic mesh is for porous medium flow, and the four black vertical thin rectangles are for heat pipes (only the condenser section is shown). The red 'x' is a nearest point that bridges the data transfer between the master and sub App's.

The coupling between the 2D heat structure (heat pipes) and 3D porous medium flow equations are again realized by data transfer between the master and sub App's. The coolant fluid temperature is transferred from the masterApp to the subApp using MOOSE's built-in object 'NearestPointLayeredAverage', which will be used as boundary condition to compute convective heat flux on heat pipe surfaces. The heat pipe wall heat flux is transferred back from the subApp to the masterApp using MOOSE's built-in object 'NearestPointLayeredSideFluxAverage', which will be converted to volumetric heat source to the porous medium flow energy equation. A list of nearest point coordinates is therefore required to bridge data transferring between the two App's. As shown in Figure 10, the red 'x' represents one of such nearest points for this unit cell, which is arranged in the center of the cell.

As a short discussion, this current mesh-based coupling and data transfer algorithm is still quite far from being generic. This current approach implies that the 2D heat structures are straight and follow regular patterns. It also requires additional information of the mesh for porous medium flow, or even certain level of manipulation during mesh generation, such that the list of nearest points could be correctly generated/obtained. If more complex geometries, for example curved heat structures and irregular shapes of the porous medium zone, are to be modeled, a more generic approach should be considered. The work presented in [10] is such an example, which however requires significant effort to develop the data mapping methodology, and is not considered in this current work scope.

As for SAM simulation, the heat exchanger is a simple rectangular prism of the size of 3m (x) × 0.76m (y) × 0.5m (z). The coolant is helium with an inlet velocity of 10 m/s, and outlet

pressure of 1 MPa. All heat pipes are identical, which is 2m long, with a 1m long evaporator section, a 0.5m long adiabatic section, and a 0.5m long condenser section, and the outer diameter is 0.034m. A uniform heat flux, 10^5 W/m^2, is applied to the evaporator section of all heat pipes.

Steady-state SAM simulation result is shown in Figure 11. Fluid temperature stays at the same in the inlet cavity zone, and then increases linearly in the porous zone as a result of heat transfer, then stays at the same in the outlet cavity zone. Solid temperature also shows a similar trend, which increases from left to right as the fluid temperature increases. A more detailed heat structure temperature distribution is given in Figure 12, from which it can be observed that the largest temperature gradients are in the wall and wick region of both evaporator and condenser sections, while the vapor core temperature is almost constant. More details on heat pipe simulation capability of SAM and its application in modeling heat pipe cooled reactors could be found in [11] and [12].

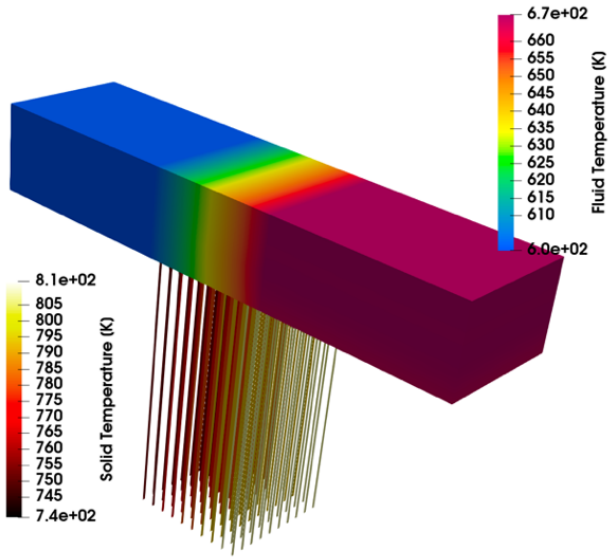

Figure 11, SAM simulation results of 2D heat structures coupling with 3D porous medium flow problem

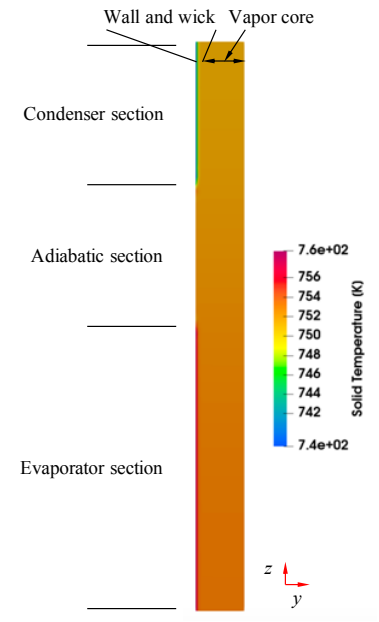

Figure 12, Heat structure temperature distribution in a heat pipe from SAM simulation. The plot was enlarged 10 times in the y-direction for display purpose.

5 Effective Thermal Conductivity of Pebble Beds

For pebble-bed reactor designs, the decay heat removal mechanism can be quite different from that of most existing light-water reactor designs, which heavily rely on active safety systems. Instead, HTGR and PB-FHR designs are mainly relying on their passive decay heat removal mechanism that utilizes its large vessel surface area as a way of transferring decay heat. For example, during a postulated pressurized conduction cooldown (PCC) event [13][14] in HTGR, the majority of decay heat is transferred from the core region radially to reactor core vessel surface via heat conduction, and then is transferred to the Reactor Cavity Cooling System (RCCS) via thermal radiation and convection. For a given core configuration, the peak fuel temperature is thus largely dictated by the effective thermal conductivity in the core. There have been multiple experimental efforts to study such decay heat removal capability for HTGR designs. The SANA [15] experiment was performed in the 1990s in Germany to demonstrate the passive decay heat removal capability of pebble bed reactor designs, which has been widely used for code benchmark/validation purpose in nuclear reactor thermal-hydraulics community. Later, the HTTU experiment [16][17] was performed in South Africa to directly investigate the effective thermal conductivity of a prototypical pebble bed.

To support system level safety analysis of HTGR and PB-FHR applications, correlations for effective thermal conductivity of pebble bed have been implemented in SAM. Although there exist a large number of such correlations and their variances of different formulations [18], most of them share common features to account for several major heat transfer mechanisms, such as heat conduction through pebbles and pebble contact areas, heat conduction/convection through the fluid, and thermal radiation from pebble to pebble. Currently, two correlations have been selected and implemented in SAM, i.e., the Zehner, Bauer, and Schlünder (ZBS) [18][19][1] and IAEA [20] correlations.

The Zehner, Bauer, and Schlünder (ZBS) model is given as,

$$\frac{k_{eff}}{k_f} = \left(1-\sqrt{1-\varepsilon}\right)\varepsilon\left[\frac{1}{\varepsilon - 1 + \kappa_G^{-1}} + \kappa_r\right] + \sqrt{1-\varepsilon}\left[\varphi\kappa_s + (1-\varphi)\kappa_C\right] \tag{5.1}$$

Of the ZBS model, the non-dimensional effective thermal conductivity related to fluid phase conduction, κ_G, is simplified to be 1. The exact definition of this term is referred to [18] and [19]. The non-dimensional effective thermal conductivity related to thermal radiation is given as,

$$\kappa_r = \frac{4\sigma}{\frac{2}{\varepsilon_r} - 1} T^3 \frac{d_p}{k_f}$$

with ε_r being the surface emissivity, σ the Stephan-Boltzmann constant, and d_p the pebble diameter. The non-dimensional effective thermal conductivity related to solid heat conduction

[1] The original reference for the ZBS model is not available, and the ZBS model has been taken from these two references. A cross check has been done to make sure that these two sources agree with each other.

is simple $\kappa \equiv k_s/k_f$. The last contribution represents the heat transfer due to solid conduction, fluid conduction, and thermal radiation,

$$\kappa_C = \frac{2}{N}\left\{\frac{B(\kappa+\kappa_r-1)}{N^2\kappa_G\kappa}\ln\frac{\kappa+\kappa_r}{B[\kappa_G+(1-\kappa_G)(\kappa+\kappa_r)]}+\frac{B+1}{2B}\left[\frac{\kappa_r}{\kappa_G}-B\left(1+\frac{1-\kappa_G}{\kappa_G}\kappa_r\right)\right]-\frac{B-1}{N\kappa_G}\right\}$$

with

$$B = 1.25\left(\frac{1-\varepsilon}{\varepsilon}\right)^{10/9}$$

and

$$N = \frac{1}{\kappa_G}\left(1+\frac{\kappa_r-B\kappa_G}{\kappa}\right)-B\left(\frac{1}{\kappa_G}-1\right)\left(1+\frac{\kappa_r}{\kappa}\right)$$

For the IAEA model, it argues that there are several types of heat transfer mechanisms in pebble beds, including radiation in void region, conduction of gas (fluid phase), conduction of spherical and convection of gas (fluid phase). The IAEA effective thermal conductivity model includes all except for the gas phase convection part, and therefore, it includes three parts: 1) solid conduction- void radiation-solid conduction process, 2) solid conduction—gas conduction—solid conduction process, and 3) solid conduction—contact area conduction—solid conduction process. The IAEA model is thus given as,

$$k_{eff} = k_{eff}^r + k_{eff}^g + k_{eff}^c \tag{5.2}$$

The solid conduction-void radiation-solid conduction contribution to the total effective thermal conductivity is given as,

$$k_{eff}^r = \left\{\left[1-(1-\varepsilon)^{1/2}\right]\varepsilon+\frac{(1-\varepsilon)^{1/2}}{\frac{2}{\varepsilon_r}-1}\cdot\frac{B+1}{B}\cdot\frac{1}{1+\frac{1}{(2/\varepsilon_r-1)\Lambda}}\right\}4\sigma T^3 d_p \tag{5.3}$$

with

$$\Lambda = \frac{k_s}{4\sigma T^3 d_p}$$

The solid conduction—gas conduction—solid conduction contribution is given as,

$$k_{eff}^g = k_f\left\{1-\sqrt{1-\varepsilon}+\frac{2\sqrt{1-\varepsilon}}{1-B/\kappa}\left[\frac{(1-1/\kappa)B}{(1-B/\kappa)^2}\ln\frac{\kappa}{B}-\frac{B+1}{2}-\frac{B-1}{1-B/\kappa}\right]\right\} \tag{5.4}$$

The solid conduction—contact area conduction—solid conduction contribution is given as,

$$k_{eff}^c = k_s\left[\frac{3(1-\mu_p)^2}{4E_s}fR\right]^{1/3}\frac{1}{0.531S}\left(\frac{N_A}{N_L}\right) \tag{5.5}$$

with

$$f = p\frac{S_F}{N_A}$$

where N_A and N_L are the number of pebbles per unit area and length, respectively. $R = d_p/2$ is the pebble radius. For the simple cubic arrangement of pebbles,

$$S = 1$$

$$S_F = 1$$

$$N_A = 1/(4R^2)$$

$$N_L = 1/(2R)$$

For graphite, Poisson ratio $\mu_p = 0.136$ and Young's modules $E_s = 9 \times 10^9$ N/m^2 are provided as default values in current implementation. The external pressure p is related to the weight of pebbles in the pebble bed. Although an exact formula was not given in the IAEA model [20], based on the original discussion provided in [21], one could reason that such a pressure is pebble bed depth-dependent, and the pebble bed pressure can be computed as,

$$p = \rho_s g(1-\varepsilon)dz$$

where $dz = z - z_0$ is the local bed depth with respect to the bed top surface at z_0.

5.1 Validation against HTTU data

The High Temperature Test Unit (HTTU) facility, developed by the PBMR company in collaboration with the North-West University and M-Tech Industrial (Pty) Ltd. in South Africa, is an experiment facility dedicated to study the different thermal-fluid phenomena of pebble bed type of HTGR [17]. A separate effect test has been performed to investigate the effective thermal conductivity of the pebble bed.

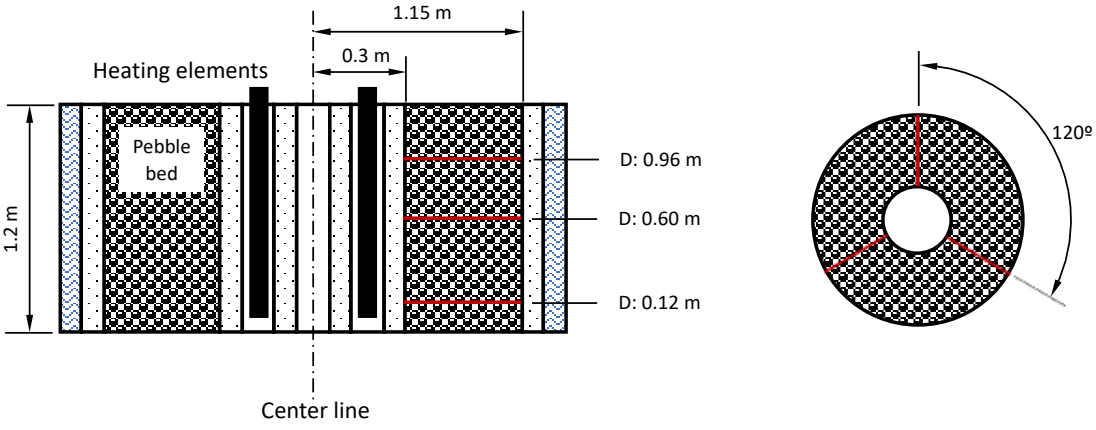

(a) (b)

Figure 13, Hight temperature test unit (HTTU): (a) vertical cut through the HTTU test section, (b) horizontal cut through the HTTU test section; and red lines for locations of thermal-couples (see Refs. [17] for more details).

As shown in Figure 13, the test facility consists of approximately 25,000 graphite pebbles randomly packed within an annular core configuration bounded by inner and outer graphite reflectors. The facility is filled with nitrogen gas at 0.1 atmospheric pressure to reduce heat transfer due to gas natural convection. A set of heater elements/electrodes are inserted in the inner graphite reflector region to provide heat to the pebble bed, while the outer reflector was enclosed within a water-cooled jacket, which removes the heat. The top and bottom of the pebble bed was well thermally insulated to limit heat loss. Pebble surface temperatures are measured at multiple vertical and circumferential locations. In [17], these temperature measurements were used to derive the effectively thermal conductivity of the pebble bed based on the Fourier's law. Two test cases, namely the 82kW and 20kW cases, have been selected to validate SAM's implementation of effective thermal conductivity correlations described previously in this section.

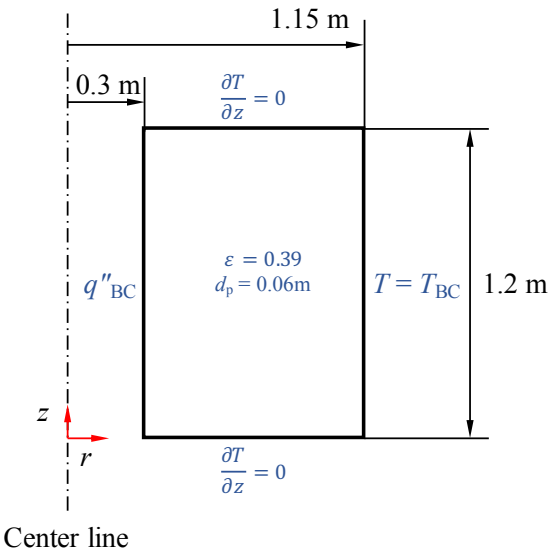

Figure 14, 2D RZ domain and boundary conditions for HTTU simulation using SAM.

For SAM validation purpose, we take advantage of the axial symmetry of the test facility, and thus the pebble bed could be simplified using a 2D RZ domain, with uniformly distributed porosity 0.39 and constant pebble diameter 0.06m, as shown in Figure 14. As the main purpose is to validate the effective thermal conductivity correlations, SAM simulations have been simplified compared to experiments. Some discussions on the simplifications are provided as follows. Although top and bottom thermal insulation was installed, there were still some level of heat loss from these two surfaces, and thus the radial heat transfer rate, Q in kW, is not constant along the radial direction, see figures 15 and 16 of [17]. The heat loss is estimated to be approximately 2-3% and is not considered in SAM simulations. As shown in Figure 14, zero temperature gradient boundary conditions are still used for the top and bottom surfaces. For each test cases (82kW or 20kW), there were two experimental tests performed and the total heat transfer rate is slightly off from each other, also in the range of 1-2% [17]. An averaged

heat transfer rate is thus used to compute the heat flux at the inner boundary of the simulated domain. This averaged value is simply computed as an arithmetic mean as,

$$Q_{avg} = \frac{Q_{max,test\ 1} + Q_{min,test\ 1} + Q_{max,test\ 2} + Q_{min,test\ 2}}{4}$$

On the outer surface, a simplification is made in SAM simulations to use a Dirichlet type of boundary condition to directly set the wall temperature. This is justified by the fact that measured temperatures on this outer surface are quite identical to each other, although a small level of scattering was also observed, and that the main validation purpose is on the effective thermal conductivity in the pebble bed. The wall temperature on the outer surface, T_{BC}, is also computed as an arithmetic average of all measured temperatures. These input parameters for SAM simulations are summarized Table 2.

Thermal conductivity of the graphite is approximated as piece wise linear function of solid temperature that was digitized from figure 26 of [17]. The values are listed in Table 3. A constant density, 1673 kg/m^3, is used for graphite, which is taken from measurements 3 of [15]. Thermal conductivity of nitrogen at 0.1 atmospheric pressure is also approximated as piece wise linear function of fluid temperature. The values are computed from the NIST website [22] and are listed in Table 4.

Table 2 Input parameters for SAM HTTU validation

	82kW Case	20kW Case
Heat rate [kW]	66.27	11.92
q''_{BC} [W/m^2]	29298.14	5267.73
T_{BC} [°C]	104.57	46.67

Table 3 Graphite thermal conductivity as a function of temperature, digitized from figure 26 of [17]

Temperature [K]	Thermal conductivity [W/(m-K)]
288.09	154.90
365.28	138.40
465.98	120.17
572.07	104.18
666.29	92.49
767.49	82.18
867.05	74.44
970.46	67.91
1071.47	63.27
1164.63	59.66
1271.85	56.22
1471.40	50.37

Steady-state results were then obtained from both cases using a uniform 40(r)×20(z) mesh size. SAM-predicted pebble surface temperatures are plotted against experimental data in Figure 15 for the 82kW case and Figure 16 for the 20kW case, respectively. SAM-predicted results are sampled from the vertical center of the domain, i.e., z = 0.6m, while experimental data are taken from vertical location C at the same axial location. For the 82kW case, SAM-predicted temperatures using the IAEA and ZBS correlations agree pretty well with experimental data. For the 20kW case, the IAEA correlation produces slightly better prediction on pebble surface temperature, while the ZBS correlation produces higher temperatures than experiments. It can also be observed that temperature gradient near the inner and outer surfaces are larger for experimental data compared with SAM-predicted results, e.g., using IAEA correlation. This indicates that IAEA correlation predicts a larger effective thermal conductivity than experimentally observed. The main reason is probably due to that a uniform porosity is used in the SAM simulation, while in reality, porosity near walls are generally larger than the so-called bulk porosity, which would effectively reduce local effective thermal conductivity. This is also evident as shown in Figure 17, in which the SAM- predicted effective thermal conductivity values using the IAEA correlation are plotted against those derived from temperature measurements. Clearly, the near wall effect is significant. It has not been considered in this work, and will be included in future studies. Nevertheless, overall, the IAEA model shows a pretty good agreement with experimental data when predicting effective thermal conductivity of the pebble bed.

Table 4 Nitrogen thermal conductivity as a function of temperature. Source: NIST website [22]

Temperature [K]	Thermal conductivity [W/(m-K)]
300	0.025831
400	0.032183
500	0.038125
600	0.043902
700	0.049592
800	0.055186
900	0.060656
1000	0.065982
1100	0.071152
1200	0.076166
1300	0.081031
1400	0.085757
1500	0.090355

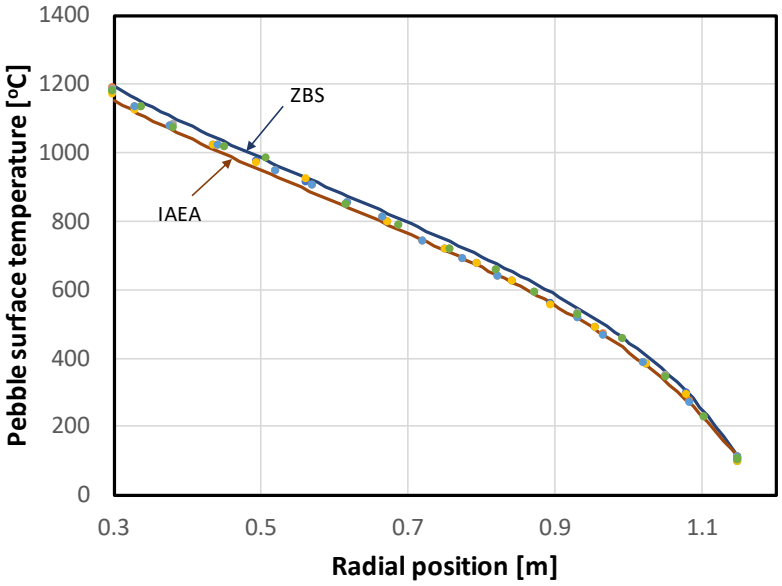

Figure 15, SAM-predicted pebble bed temperature compared with experimental data for the 82kW case.

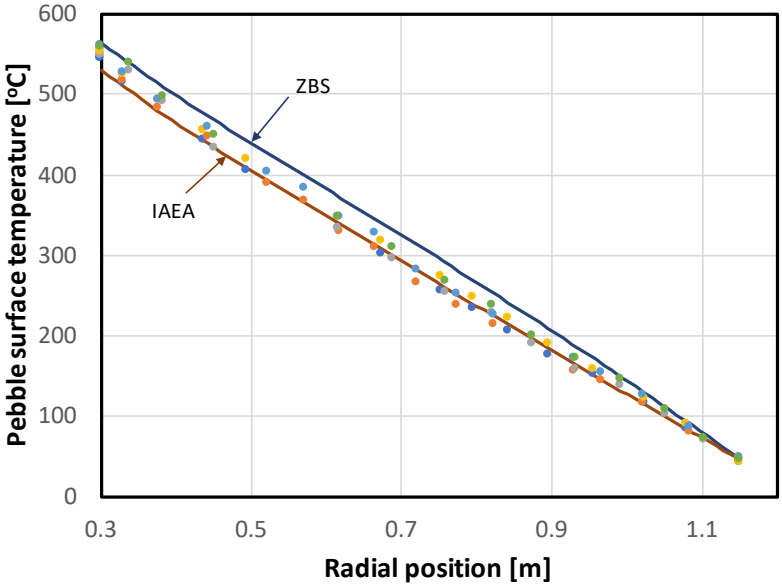

Figure 16, SAM-predicted pebble bed temperature compared with experimental data for the 20kW case.

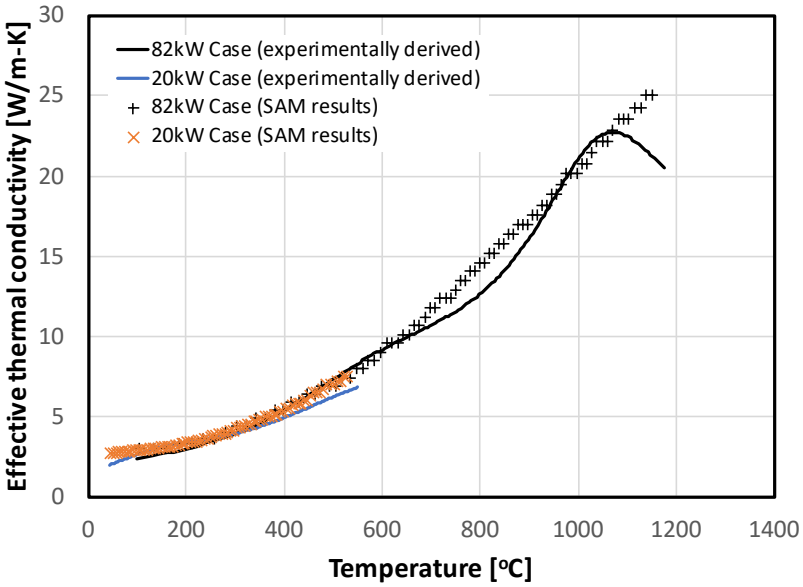

Figure 17, Effective thermal conductivity: SAM-predicted values using IAEA model compared with those derived from temperature measurements based on the Fourier's law [17].

6 Summary

This report summarizes recent SAM code improvement to heat transfer modeling capabilities to support system and core thermal-hydraulics analysis for advanced non-LWRs. The purpose of these new capabilities is to address the thermal-hydraulics analysis challenges to consider multi-scale, multi-dimensional, and multi-physics effects in advanced non-LWRs. Recent SAM code improvements have been made to address these modeling and simulation challenges, which include the implementation of energy equation for solid structure in porous medium and its coupling with porous medium flow equations; coupling between one-dimensional flow equation and three-dimensional heat conduction equation; coupling between two-dimensional heat structure and three-dimensional porous medium flow equations; and implementation of effective thermal conductivity of solid pebble beds and its validation against High Temperature Test Unit (HTTU) experimental data. Demonstration or validation test problems are also included in this report to confirm the successful implementation of these capabilities.

Acknowledgement

This report was prepared as an account of work sponsored by an agency of the U.S. Government. Neither the U.S. Government nor any agency thereof, nor any of their employees, makes any warranty, expressed or implied, or assumes any legal liability or responsibility for any third party's use, or the results of such use, of any information, apparatus, product, or process disclosed in this report, or represents that its use by such third party would not infringe privately owned rights. The views expressed in this paper are not necessarily those of the U.S. Nuclear Regulatory Commission.

The authors sincerely thank Mr. Joseph Kelly at U.S. Nuclear Regulatory Commission for the fruitful discussions throughout the work and for providing help to the implementation of effective thermal conductivity correlations. The authors would also greatly appreciate intern students Brent Hollrah and Michael Gorman of Texas A&M University and Guojun Hu of Argonne National Laboratory for their support to this study, and Professor Pieter Rousseau of University of Cape Town for providing HTTU temperature measurement.

Reference

[1] Hu, R., *SAM Theory Manual*, Nuclear Engineering Division, Argonne National Laboratory, ANL/NE-17/4, Argonne, IL, March, 2017.

[2] U.S.NRC. NRC Non-Light Water Reactor (Non-LWR) Vision and Strategy, Volume 1 – Computer Code Suite for Non-LWR Design Basis Event Analysis. Technical report, U.S. NRC, 2019.

[3] S. Struth. Thermix-Direkt: Ein Rechenprogramm zur instationaren zweidimensionalen Simulation thermohydraulischer Transienten. Technical report, Forschungszentrum Julich, 1995.

[4] April J. Novak, Ling Zou, John W Peterson, David Andrs, Joe Kelly, Rachel N. Slaybaugh, Richard C. Martineau, and Hands D. Gougar. Pronghorn theory manual. Technical Report INL/EXT-18-44453, Idaho National Laboratory, 2018.

[5] W. T. Sha, H. M. Domanus, and R. C. Schmitt. COMMIX-1: A Computer Program for Three- Dimensional, Transient, Single-Phase Thermal-Hydraulic Analysis. Technical Report NUREG-0415, ANL-77-96, Argonne National Laboratory, 1978.

[6] W. T. Sha. Novel Porous Media Formulation for Multiphase Flow Conservation Equations. Cambridge University Press, 2011.

[7] Han Young Yoon, Jae Ryong Lee, Hyungrae Kim, Ii Kyu Park, Chul-Hwa Song, Hyoung Kyu Cho, and Jae Jun Jeong. Recent Improvements in the CUPID Code for a Multi-Dimensional Two- Phase Flow Analysis of Nuclear Reactor Components. *Nuclear Engineering and Technology*, **46**(5):655–666, 2014.

[8] Rui Hu. Three-dimensional flow model development for thermal mixing and stratification modeling in reactor system transients analyses. *Nuclear Engineering and Design*, **345**:209–215, 2019.

[9] Nuclear Safety Standards Commission (KTA). Reactor Core Design of High-Temperature Gas- Cooled Reactors Part 2: Heat Transfer in Spherical Fuel Elements. Technical Report KTA 3102.2, Nuclear Safety Standards Commission, 1983.

[10] A. Toti, J. Uribe, M. Rabbitt, C. Sigournay, J. Pethan, S. Pandit, and P. Brown. Thermal-hydraulic Simulation of Advanced Gas-cooled Reactors Steam Generators using Coupled Porous CFD and 1D Two-phase Flow Modeling. In 18th International Topical Meeting on Nuclear Reactor Thermal Hydraulics - NURETH, 2019.

[11] G. Hu, R. Hu, and L. Zou. Development of Heat Pipe Reactor Modeling in SAM. Technical report ANL/NSE-19/9, Argonne National Laboratory, 2019.

[12] G. Hu, R. Hu, J. M. Kelly, and J. Ortensi. Multi-Physics Simulations of Heat Pipe Micro Reactor. Technical report ANL/NSE-19/25, Argonne National Laboratory, 2019.

[13] Prasad Vegendla, Rui Hu, and Ling Zou. Modeling and Simulations of HTGR during Pressurized Conduction Cooldown Transients Using SAM Code. In 2019 American Nuclear Society Winter Meeting and Nuclear Technology Expo, 2019.

[14] Prasad Vegendla, Rui Hu, and Ling Zou. Multi-Scale Modeling of Thermal-Fluid Phenomena Re- lated to Loss of Forced Circulation Transient in HTGRs. Technical Report ANL-19/35, Argonne National Laboratory, 2019.

[15] B. Stocker and H. Nieben. Data Sets of the SANA Experiment 1994-1996. Technical report JUEL--3409, Forschungszentrum Jülich, 1996.

[16] P. G. Rousseau and M. van Staden. Introduction to the PBMR heat transfer test facility. *Nuclear Engineering and design*, **238**(11):3060–3072, 2008.

[17] P. G. Rousseau, C. G. du Toit, W. van Antwerpen, and H. J. van Antwerpen. Separate effects tests to determine the effective thermal conductivity in the PBMR HTTU test facility. *Nuclear Engineering and Design*, **271**:444–458, 2014.

[18] W. van Antwerpen, C. G. du Toit, and P. G. Rousseau. A review of correlations to model the packing structure and effective thermal conductivity in packed beds of mono-sized spherical particles. *Nuclear Engineering and design*, **240**(7):1803–1818, 2010.

[19] Ersheng You, Ximing Sun, Fubing Chen, Lei Shi, and Zuoyi Zhang. An improved prediction model for the effective thermal conductivity of compact pebble bed reactors. *Nuclear Engineering and Design*, **323**:95–102, 2017.

[20] IAEA. Heat Transport and Afterheat Removal for Gas Cooled Reactors Under Accident Conditions. Technical report IAEA-TECDOC-1163, International Atomic Energy Agency, 2000.

[21] C. K. Chan and C. L. Tien. Conductance of packed spheres in vacuum. *Journal of Heat Transfer*, **95**:302–308, 1973.

[22] NIST. NIST Chemistry WebBook, SRD 69. https://webbook.nist.gov. Accessed: 2019-10-10.

Nuclear Science and Engineering Division
Argonne National Laboratory
9700 South Cass Avenue, Bldg. 208
Argonne, IL 60439

www.anl.gov

Argonne National Laboratory is a U.S. Department of Energy
laboratory managed by UChicago Argonne, LLC